

DECLASSIFIED

N65-28462  
(ACCESSION NUMBER)

NA

FACILITY FORM 802

31  
(PAGES)

(THRU)

6  
(CODE)

(NASA CR OR TMX OR AD NUMBER)

C1  
(CATEGORY)

NACA RM E56K15

# RESEARCH MEMORANDUM

DECLASSIFIED BY AUTHORITY OF NASA  
CLASSIFICATION CHANGE NOTICES NO. 10  
DATED 5-24-65 ITEM NO. 1

PERFORMANCE OF TWIN-DUCT VARIABLE-GEOMETRY SIDE

INLETS AT MACH NUMBERS OF 1.5 TO 2.0

By Richard A. Yeager, Milton A. Beheim, and John L. Klann

Lewis Flight Propulsion Laboratory

Cleveland, Ohio

DECLASSIFIED BY AUTHORITY OF NASA  
CLASSIFICATION CHANGE NOTICES NO. 10  
DATED 5-24-65 ITEM NO. 1

DECLASSIFIED: EFFECTIVE 4-29-65  
AUTHORITY F.G. DROBKA (ATSS\*  
MEMO dated 5-13-65:AFSDO 5439

GPO PRICE \$ \_\_\_\_\_

OTS PRICE(S) \$ \_\_\_\_\_

Hard copy (HC) 2.50

Microfiche (MF) 2.00

## NATIONAL ADVISORY COMMITTEE FOR AERONAUTICS

WASHINGTON

January 21, 1957

RESEARCH MEMORANDUM

## PERFORMANCE OF TWIN-DUCT VARIABLE-GEOMETRY SIDE

## INLETS AT MACH NUMBERS OF 1.5 TO 2.0

By Richard A. Yeager, Milton A. Beheim, and John L. Klann

## SUMMARY

28462

The performance of a twin-duct air-intake system mounted on the sides of a 1/8-scale fuselage forebody model of a proposed aircraft was investigated at free-stream Mach numbers of 1.5 to 2.0 over a range of angles of attack and yaw. The inlets were of the double-ramp type and were tested at  $0^\circ$  and  $-5^\circ$  cant with respect to the fuselage centerline. The test was conducted with several second-ramp angles and at several second-ramp longitudinal positions along the first-ramp surface. Various methods of second-ramp surface boundary-layer removal were also investigated.

For a particular second-ramp position a slot in the second ramp inside the cowl increased the subcritical stability over that obtained without boundary-layer removal, while perforations in the second ramp just upstream of the cowl had no effect on stability. Little change in pressure recovery was obtained by employing either method of boundary-layer control. Canting the inlets from  $0^\circ$  to  $-5^\circ$  improved the total-pressure recovery at positive angles of attack greater than  $2^\circ$  and increased subcritical stability at all the Mach numbers investigated. At Mach number 2.0 and  $2^\circ$  angle of attack, the  $-5^\circ$ -cant inlet yielded a peak pressure recovery of 86 percent and a critical mass-flow ratio of 84 percent with 28 percent stability. The distortion was about 7 percent for critical and subcritical operation. Asymmetrical duct flow occurred only during operation where normal-shock oscillations were observed at angle of attack but for all operating conditions at angle of yaw. The addition of canards on the fuselage upstream of the  $0^\circ$ -cant inlets increased the total-pressure recovery and reduced distortion at all positive angles of attack.

*Author*

## INTRODUCTION

An investigation has been conducted in the Lewis 8- by 6-foot supersonic wind tunnel to determine the performance of a twin-duct air-intake system mounted on the sides of a 1/8-scale fuselage forebody model of a proposed aircraft. The fuselage inlet configuration differed from that



previously reported in references 1 and 2 in that the fuselage cross section at the inlet station was more nearly triangular and the inlets were mounted nearer the top of the fuselage and farther downstream from the canopy. The double-ramp inlets were tested at  $0^\circ$  and  $-5^\circ$  cant with respect to the fuselage centerline. Several second-ramp angles, several second-ramp longitudinal positions along the first-ramp surface, and various methods of second-ramp surface boundary-layer removal were employed. In addition, for a portion of the test, canard surfaces were mounted on the fuselage upstream of the  $0^\circ$ -cant inlets.

The test was conducted over a range of angles of attack and yaw at free-stream Mach numbers of 1.5 to 2.0.

#### SYMBOLS

The following symbols are used in this report:

$A_{in}$  inlet capture area: 16.42 sq in. for  $0^\circ$  cant, 15.61 sq in. for  $-5^\circ$  cant

$A_{ref}$  reference area (model station 70.61), 80.10 sq in.

$C_D$  axial component of drag coefficient based on  $A_{ref}$

$M$  Mach number

$m_3/m_0$  ratio of inlet mass flow to mass flow at free-stream conditions through inlet capture area,  $A_{in}$

$P$  total pressure

$p$  static pressure

$\alpha$  model angle of attack, deg

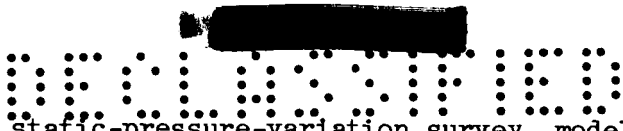
$\epsilon$  second-ramp extension, in.

$\psi$  model angle of yaw, deg

Subscripts:

0 free stream

1 inlet survey, model station 34.78



- 2 diffuser static-pressure-variation survey, model station 48.91
- 3 compressor-face station, model station 64.97

APPARATUS AND PROCEDURE

General Arrangement

A photograph and a schematic diagram of the model are presented in figures 1(a) and (b), respectively. The fuselage nose was drooped  $4^\circ$  with respect to the fuselage centerline to aid pilot vision rather than to influence inlet performance. Because of armament storage, a rather sharp bend was necessary in the ducts near model station 55 (fig. 1(b)) just upstream of their junction.

The compression ramps of the inlets were raised above the fuselage boundary layer; and a combination scoop and diverter, illustrated in figure 1(b), captured a portion of this boundary layer and diverted the remainder. The flow of the captured boundary layer was controlled with individual exit plugs and was exhausted at the base of the model. Main diffuser airflow was also plug-controlled. The inlets were investigated with the centerline of the initial portion of the duct aligned with the fuselage centerline ( $0^\circ$ -cant inlets) and also inclined downward  $5^\circ$  ( $-5^\circ$ -cant inlets). For a part of the test the canard surfaces were mounted low on the fuselage beneath the canopy as shown in figure 1(b).

Inlet Details

Figures 1(c) and (d) present a photograph and a schematic diagram, respectively, of one of the inlets. The leading edge of the fixed-angle ( $9^\circ$ ) first ramp was positioned so that the first oblique shock was placed near the cowl lip at a Mach number of 2.0. The position of the leading edge of the second ramp was varied along the surface of the first. The unextended position ( $\epsilon = 0$ , see fig. 1(d)) was such that, for a second-ramp angle of  $19^\circ$ , the second oblique shock theoretically would be at the cowl lip at a Mach number of 2.0. Several second-ramp angles were investigated, each calculated to position the second oblique shock at the cowl lip for a particular design Mach number with  $\epsilon = 0$ . These were as follows:

Second-ramp angle, deg	Design Mach number
21	2.1
19	2.0
17	1.9
13	1.7
9	1.5



4151  
CHECK

In addition, second-ramp angles of  $0^\circ$  and  $30^\circ$  were tested as a means of obtaining low stable mass-flow ratios at high Mach numbers.

Compression-surface boundary layer could be removed through perforations in the second ramp just ahead of the cowl. The perforations were aligned in successive rows in the flow direction for the  $0^\circ$ -cant inlet and staggered so that alternate rows were aligned for the  $-5^\circ$ -cant inlet. In addition, a flush slot in the second ramp just inside the cowl and a combination of this slot and the perforations were investigated with the  $0^\circ$ -cant inlet. This configuration can be seen in figure 1(c). Bleed air entered the fuselage cavity and was exhausted at the base of the model.

The effect of second-ramp angle on subsonic-diffuser area variation is shown in figure 2. Duct cross sections are also indicated.

#### Instrumentation and Data Reduction

To determine the local flow conditions just upstream of the inlets, two rakes with static- and total-pressure instrumentation (see figs. 3 and 4) were mounted on the fuselage at model station 34.78 ahead of one of the inlets, and two  $6^\circ$ -half-angle wedges with total- and surface static-pressure instrumentation were mounted at the same model station ahead of the other inlet. The Pitot and static-pressure profiles obtained from the rake data were used to compute the local total-pressure profile. The wedge data were used to determine local Mach number ahead of the inlets and local flow angularity with respect to the plane of the wedges. This plane was normal to the fuselage surface and parallel to the fuselage centerline. Some data were obtained with two total-pressure rakes just inside each cowl at model station 41.00 with wall static-pressure orifices at the ends of each rake. These rakes were used to obtain the total-pressure profile at the entrance of the duct to aid in selecting a position for a Mach number sensor for second-ramp control. Each duct was instrumented at model station 48.91 to record the static-pressure variation during unstable operation.

At the compressor-face station (model station 64.97), six equally spaced rakes were employed. Each rake consisted of four total-pressure tubes arranged for area-weighted averages and an additional tube located immediately adjacent to the outer wall. Air distortion was computed from all the total tubes, and pressure recovery was obtained from an average of those tubes arranged for area-weighted averages. Downstream of these rakes at model station 71.11 were located eight static-pressure orifices, four in the outer wall and four in the centerbody. Mass-flow calculations were made using the average static pressure obtained from these orifices with the assumptions of a choked geometrical minimum area determined at the duct exit by plug position and a plug discharge coefficient of 0.99.

The two boundary-layer bleed ducts used to capture some of the fuselage boundary layer were each instrumented at model station 66.87 with a three-tube total-pressure rake and two wall static-pressure orifices. Mass-flow calculations were made from these measurements.

The axial force on the model was measured with an internal strain-gage balance system with the  $0^\circ$ -cant inlets only.

## RESULTS AND DISCUSSION

### Inlet Survey

Local flow angularity and Mach number were computed at the two positions on each of the wedges. These four values for Mach number and angularity were averaged and are presented as a function of free-stream Mach number for several angles of attack in figure 3(a). For the yaw data shown in figure 3(b), the four values of Mach number were averaged and the two values of angularity for each wedge were averaged. These data indicate that the average local Mach number ahead of the inlet did not vary appreciably for angles of attack up to  $5^\circ$  nor for angles of yaw and was always higher than the free-stream value. In addition, the local flow angularity with respect to the plane of the wedges was always more positive than the model angle of attack. At angle of yaw the upper wedge indicated a higher flow angularity than the lower wedge. (The wedges were on the windward side of the fuselage for positive angles of yaw.)

The survey-rake data (fig. 4) indicate that for all positive angles of attack the fuselage boundary layer thickened ahead of the upper portion of the inlet; at angles of yaw it thickened ahead of the bottom portion of the lee inlet. In both cases the position of the first-ramp leading edge shows that the thickening effect was sufficient to cause some boundary-layer air to enter the inlet. This can also be seen in figure 5 from the profiles of the  $0^\circ$ -cant inlets, where low recovery air is present near the ramp surface for these conditions. Some typical compressor-face profiles are also shown in this figure.

### Compression-Surface Boundary-Layer Removal and Effects of Second-Ramp Position

The effect of compression-surface boundary-layer removal on the diffuser airflow characteristics with  $\epsilon = 0$  is shown in figure 6. As shown, the slot configuration considerably increased the subcritical stability range over that obtained without boundary-layer bleed, while the perforations had no effect on stability. Both configurations slightly increased the total-pressure recovery over the no-bleed case, with a



slight decrease in critical mass-flow ratio. Although data are not presented, increasing the number of rows of perforations from 6 to 10 rows also reduced critical mass-flow ratio without affecting other performance characteristics.

The effect of second-ramp position on performance with the slot boundary-layer-removal system is presented in figure 7 for  $2^\circ$  angle of attack. As the second ramp was translated upstream along the surface of the first, an increase in total-pressure recovery was obtained; however, the critical mass-flow ratio and the subcritical stability range were decreased considerably.

The combined effects of compression-surface boundary-layer control and second-ramp position are summarized for  $2^\circ$  angle of attack in figure 8(a) and for  $0^\circ$  angle of attack in figure 8(b). The most important points to be made are as follows:

- (1) Pressure recovery was essentially independent of type of bleed.
- (2) The range of stable mass flows was greatest for the slot alone (fig. 8(a)).
- (3) Increasing second-ramp extension increased pressure recovery. At an angle of attack of  $2^\circ$  this was accompanied by a reduction in critical mass flow (fig. 8(a)). At  $0^\circ$ , however, mass flow was independent of ramp extension for extensions less than 0.25 inch.

Although not shown, the effects on distortion of varying the method of boundary-layer removal or translating the second ramp were small.

#### Instability

During the investigation two types of inlet subcritical instability were determined. As the mass-flow ratio was decreased from the critical value, the normal shocks of both inlets moved upstream of the inlets uniformly and in a stable manner until at a particular mass-flow ratio twin-duct asymmetry began to occur. The instrumentation inside the inlet showed that, as the mass flow was further reduced, the normal shock of one inlet continued to move gradually upstream while the other normal shock gradually moved back into the inlet. During operation of this type the normal shocks began to oscillate locally, resulting in small variations in diffuser pressures which gradually increased in amplitude. This instability, which will be referred to as flutter, is indicated in succeeding figures by a flagged symbol. Eventually, as the mass flow was decreased even further, inlet buzz occurred, during which the normal shocks oscillated over large distances with a sharp rise in the amplitude of diffuser pressure variations.

  
N O T E


In general, the operating regions where either of the two types of instability occurred were easily determined from schlieren observation and transient pressure instrumentation. Occasionally, however, such as at high angles of attack, the oscillations of the normal shocks gradually increased without sudden change. Some measurements of the amplitude of static-pressure variations within the inlet were obtained while total-pressure rakes were in position just inside the cowling. The presence of these rakes occasionally had a small effect on the mass-flow-ratio limits at which instability occurred, but they did not change the general trends of the amplitude variation as instability increased. These data are indicated in figures 9(a) and 10(a) by solid symbols.

#### Effect of Cant on Inlet Performance


Performance characteristics at Mach number of 2.0 and  $\epsilon$  of 0.25 are presented for the  $0^\circ$ -cant inlet in figure 9(a) and for the  $-5^\circ$ -cant inlet in figure 9(b). Comparison of the two figures shows that canting the inlets to  $-5^\circ$  appreciably improved the inlet total-pressure recovery at positive angles of attack greater than  $2^\circ$ . For example, at  $9^\circ$  angle of attack the peak total-pressure recovery was increased from 72 percent with the  $0^\circ$  cant to 79.5 percent with the  $-5^\circ$  cant with no change in critical mass-flow ratio. At  $2^\circ$  angle of attack with the  $-5^\circ$  cant, the critical mass-flow ratio was reduced 2 percent from that obtained with the  $0^\circ$  cant, and only a slight increase in peak pressure recovery was obtained. As a further result of the  $-5^\circ$  cant, both the critical mass-flow ratio and peak pressure recovery at angles of attack less than  $2^\circ$  were reduced from the values obtained with the  $0^\circ$  cant. The range of buzz-free subcritical mass-flow ratios increased appreciably at all angles of attack with the  $-5^\circ$ -cant inlet. Distortion was about 7 percent for critical and subcritical operation with both inlet configurations. At critical operation with the  $0^\circ$ -cant inlet at  $0^\circ$  angle of attack, the axial component of the drag coefficient was about 0.17 compared with 0.21 for a similar configuration reported in reference 1.

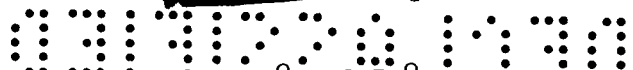
Trends similar to those obtained at a Mach number of 2.0 were obtained over the entire Mach number range investigated. The effect of changing the inlet cant at a Mach number of 1.5 is shown in figure 9(c) ( $0^\circ$  cant) and 9(d) ( $-5^\circ$  cant). At these lower Mach numbers the change in subcritical stability was small, but the pressure recovery at high angles of attack still increased.

Yaw data were obtained at a Mach number of 2.0 for both the  $0^\circ$ - and  $-5^\circ$ -cant inlets (figs. 10(a) and (b), respectively). Although the  $-5^\circ$ -cant inlets yielded slightly reduced critical mass-flow ratios, an appreciable increase in the buzz-free subcritical mass-flow range was obtained, especially for angles of yaw greater than  $3^\circ$ . Duct operation was asymmetrical at all angles of yaw.







  
 Inlet Performance with 0° and 30° Second-Ramp Angles

Second-ramp angles of 0° and 30° were investigated as a means of obtaining low stable mass-flow ratios at high Mach numbers. These data with the 0°-cant inlets appear in figure 11(a) for a Mach number of 2.0 and in figure 11(b) for a Mach number of 1.5. Similar results were obtained with the -5°-cant inlets, and data are not presented. At Mach number 2.0 with both ramp positions low buzz-free mass-flow ratios could be obtained; however, with the 0° ramp flutter was observed for all nonbuzzing operating conditions. Lower stable mass-flow ratios were available with the 30° ramp at a Mach number of 1.5. Distortion was about 5 percent with the 30° ramp for all operating conditions. For the 0° ramp the distortion was always above 7 percent and reached a maximum of 27 percent at low mass-flow ratios at Mach number of 2.0.

#### Performance with Fixed Second-Ramp Angles


The critical mass-flow ratio, the stability limits, and critical and peak total-pressure recoveries are presented as a function of free-stream Mach number for fixed second-ramp angles in figure 12. As the free-stream Mach number decreased, there was no marked change in the subcritical stability range for any one fixed ramp angle.

#### Effect of Canards

With the canard surfaces mounted on the fuselage upstream of the 0°-cant inlets, the data (fig. 13) show that for positive angles of attack the total-pressure recoveries were improved without loss in critical mass-flow ratio. The solid symbols in the figure indicate the data taken without canards (from fig. 9(a)) at angle of attack of 9°, where the largest improvement was observed. At 0° angle of attack with the same peak total-pressure recovery the critical mass-flow ratio was reduced slightly. The distortion was reduced at all positive angles of attack. The range of subcritical stability was unaffected.

#### SUMMARY OF RESULTS

An investigation was conducted to determine the performance of a double-ramp, twin-duct air-intake system mounted on the sides of a 1/8-scale fuselage forebody model of a proposed aircraft. The inlets were studied at 0° and -5° cant with respect to the fuselage centerline at free-stream Mach numbers of 1.5 to 2.0. Several second-ramp angles, several second-ramp longitudinal positions along the first-ramp surface, and various methods of second-ramp surface boundary-layer removal were tested. Some data were obtained with canards mounted on the fuselage upstream of the 0°-cant inlets. The following results were obtained:




1. With a particular second-ramp position, a slot in the second ramp just inside the cowl increased the subcritical stability over that obtained without bleed, while perforations in the second ramp just upstream of the cowl had no effect on stability. Neither method of boundary-layer removal improved pressure recovery more than 2 percent.

2. Translating the second ramp upstream along the surface of the first at  $2^\circ$  angle of attack increased the pressure recovery slightly but reduced the stable subcritical operating range. At  $0^\circ$  angle of attack, however, the increase in pressure recovery was obtained without loss in subcritical stability.

3. Canting the inlets from  $0^\circ$  to  $-5^\circ$  improved the pressure recovery at positive angles of attack greater than  $2^\circ$  at all the Mach numbers investigated. At Mach number 2.0 and  $2^\circ$  angle of attack, the  $-5^\circ$ -cant inlet yielded a peak pressure recovery of 86 percent and a critical mass-flow ratio of 84 percent with 28 percent stability. The distortion was about 7 percent for critical and subcritical operation.


4. Asymmetrical duct flow occurred only during flutter and buzz operation at angle of attack, but for all operating conditions at angles of yaw.

5. Both  $0^\circ$  and  $30^\circ$  second-ramp angles provided low, buzz-free subcritical mass-flow ratios over the Mach number range. The distortion was about 5 percent with the  $30^\circ$  ramp for all conditions, while the  $0^\circ$  ramp yielded a range from 7 to 27 percent at low mass-flow ratios at Mach number 2.0.

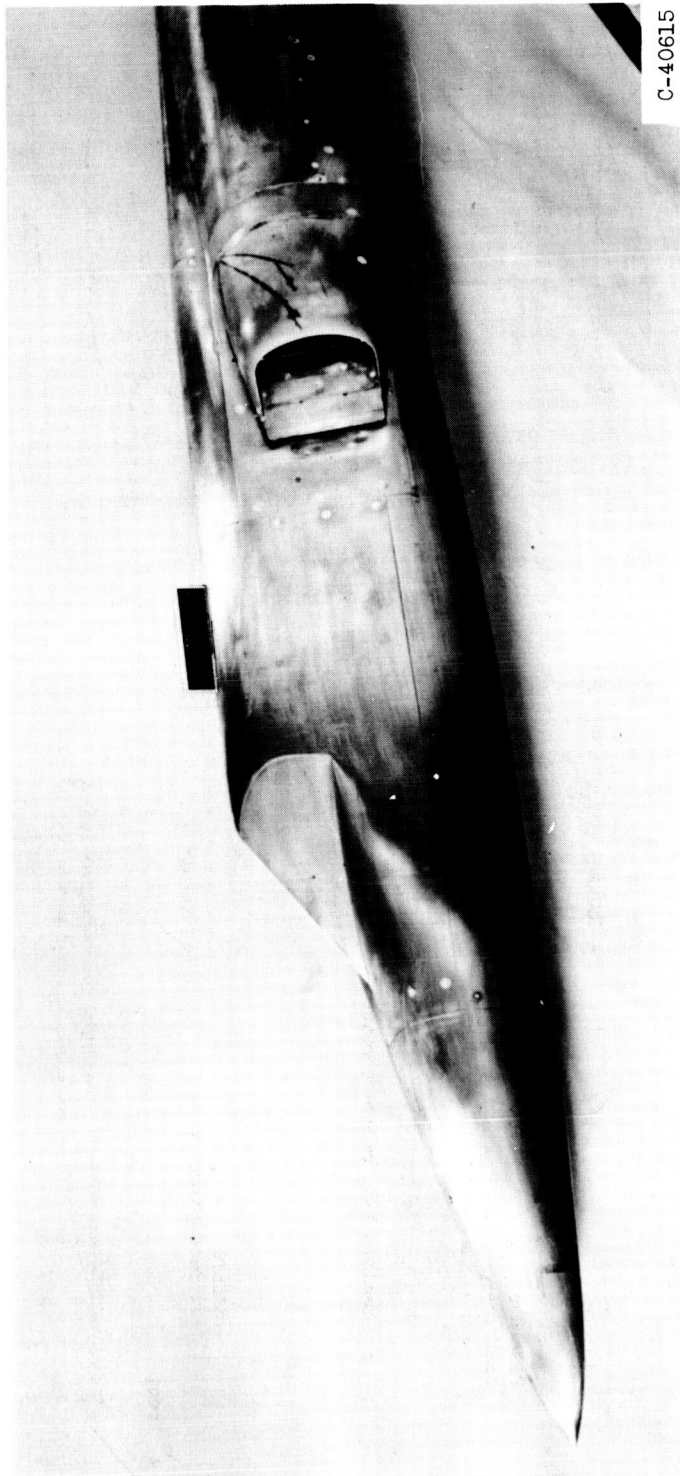
6. Addition of canards mounted on the fuselage nose upstream of the  $0^\circ$ -cant inlets increased the pressure recovery and reduced the distortion at all positive angles of attack.

Lewis Flight Propulsion Laboratory  
National Advisory Committee for Aeronautics  
Cleveland, Ohio, November 21, 1956

#### REFERENCES

1. Obery, Leonard J., Stitt, Leonard E., and Wise, George A.: Evaluation at Supersonic Speeds of Twin-Duct Side-Intake System with Two-Dimensional Double-Shock Inlets. NACA RM E54C08, 1954.
  2. Stitt, Leonard E., and Wise, George A.: Investigation of Several Double-Ramp Side Inlets. NACA RM E54D20, 1954.
- 

CONFIDENTIAL

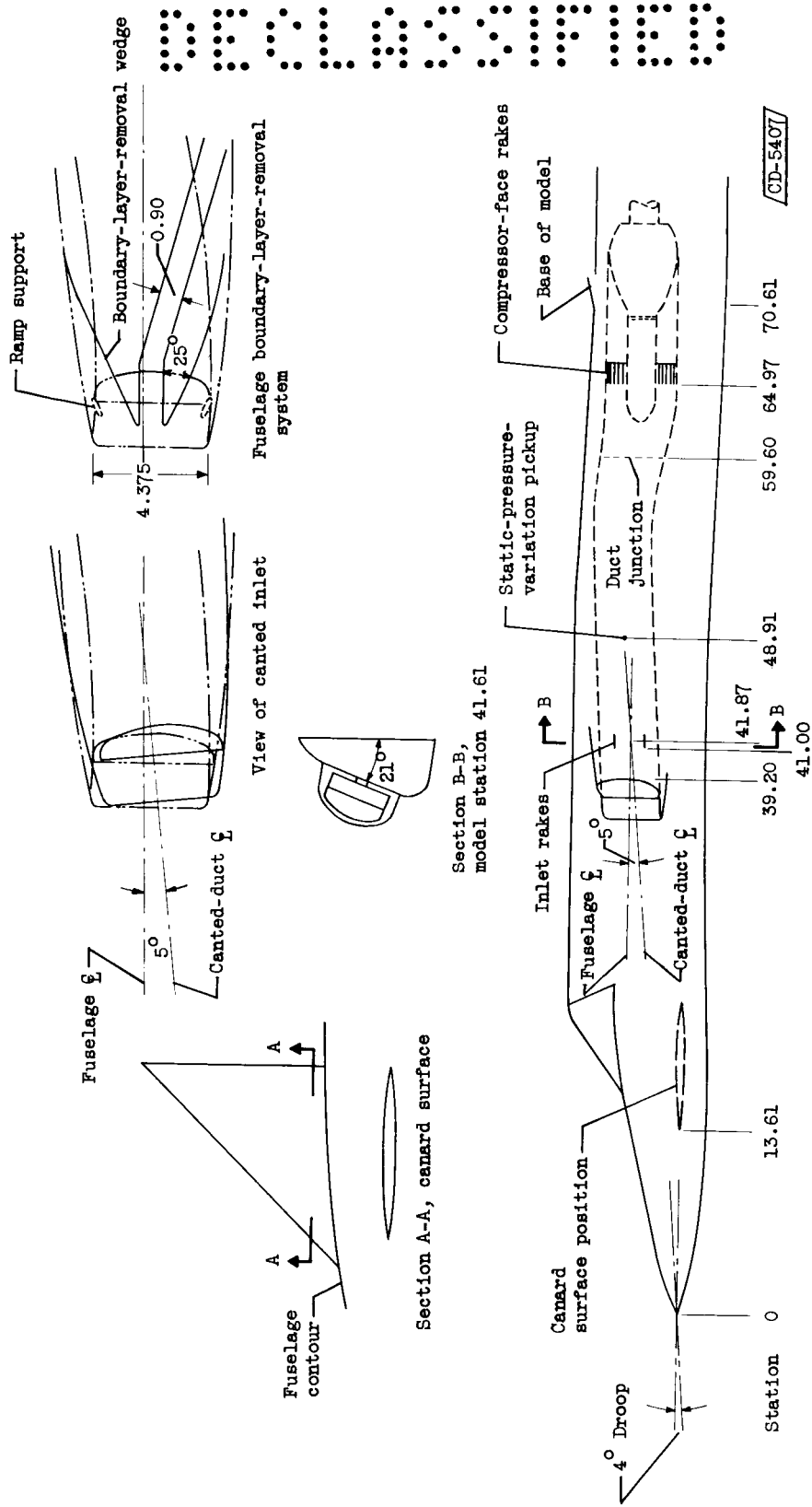


C-40615

(a) Photograph of model.

Figure 1. - Fuselage inlet model.

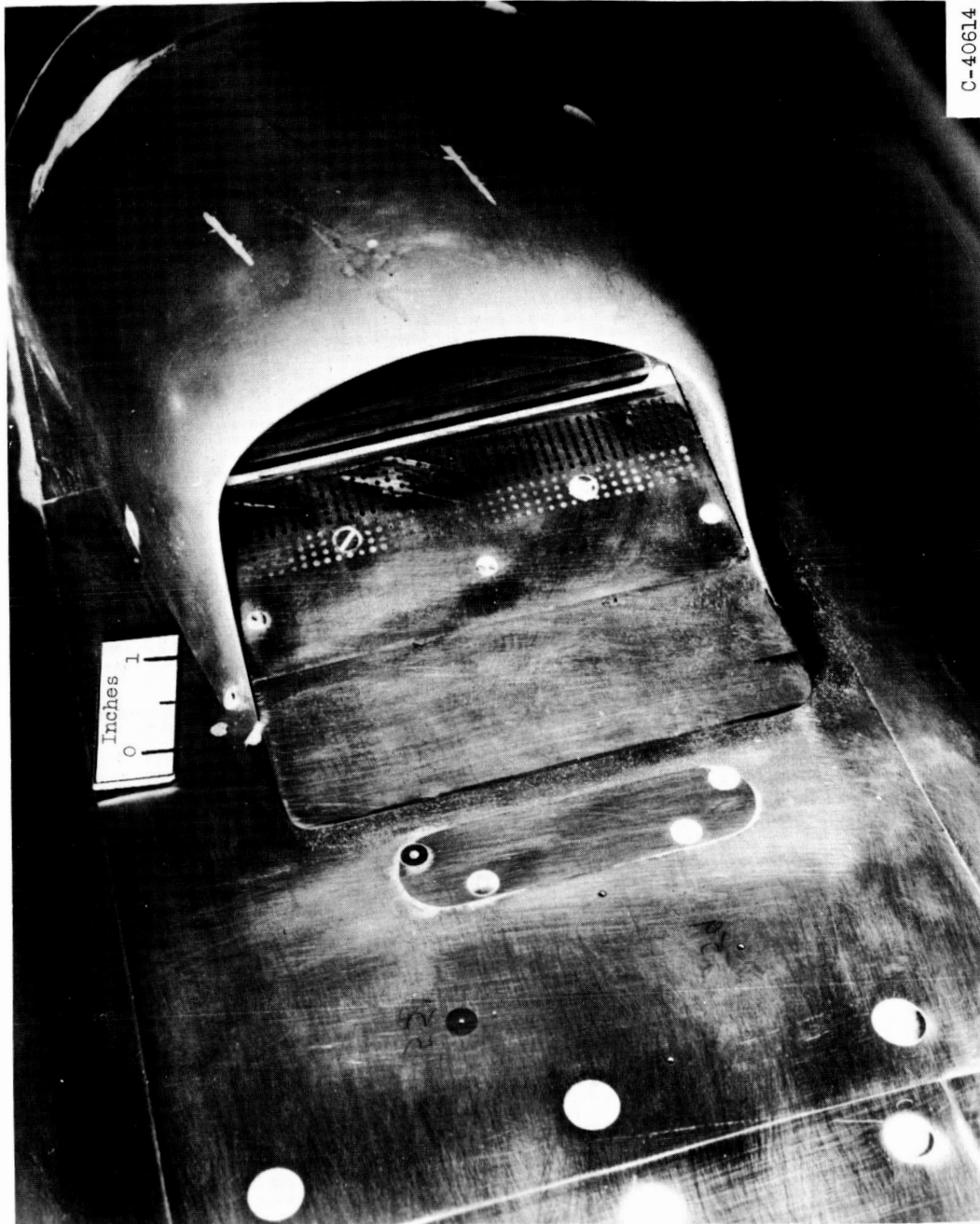
CA-2 back 4151



(b) Schematic diagram of model (all dimensions in inches).

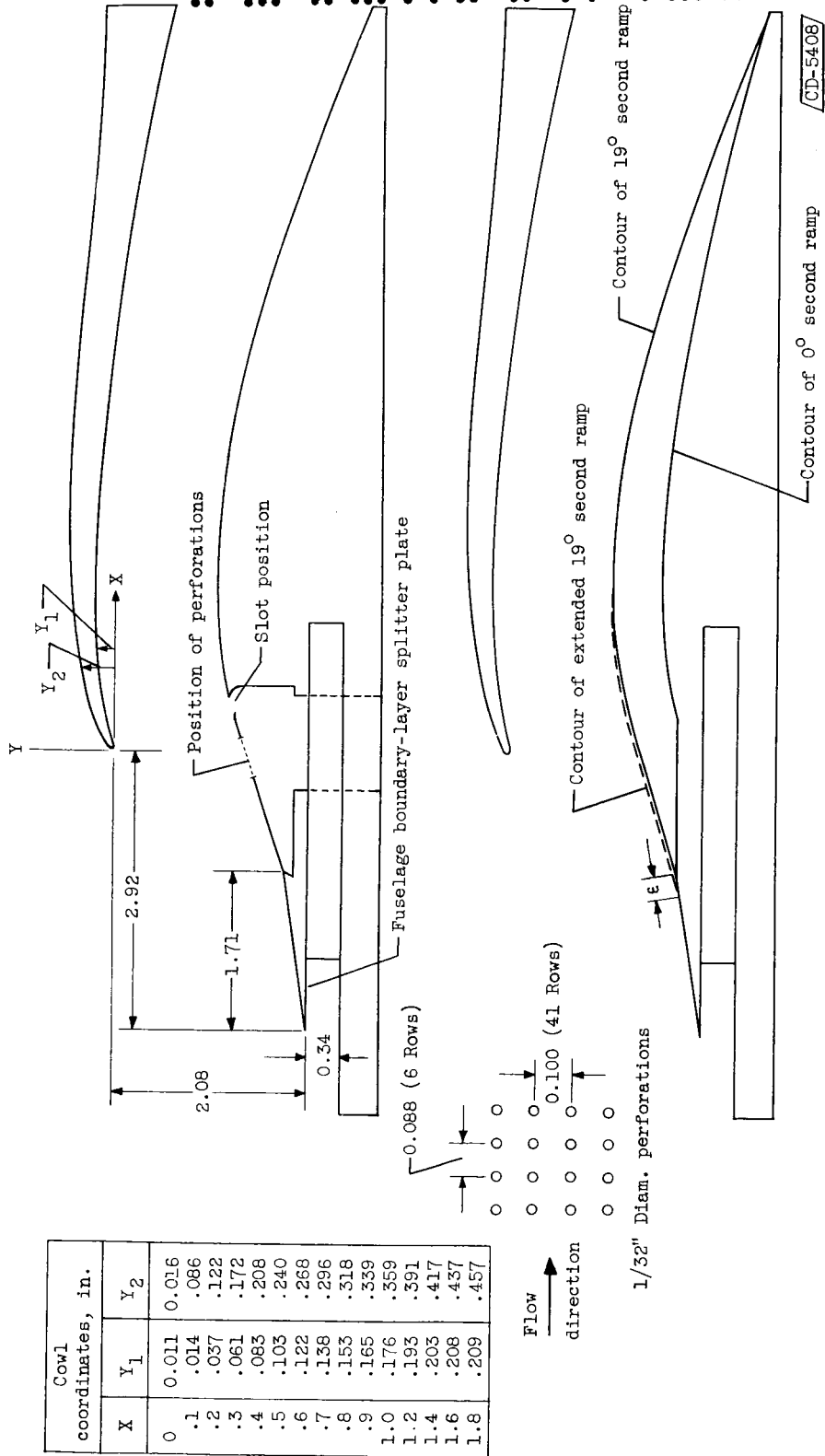
Figure 1. - Continued. Fuselage inlet model.

0371300153



(c) Photograph of inlet showing boundary-layer-control systems.

Figure 1. - Continued. Fuselage inlet model.



(d) Schematic diagram of inlet showing boundary-layer control and typical ramp contours (all dimensions in inches).

Figure 1. - Concluded. Fuselage inlet model.

4151

CONFIDENTIAL

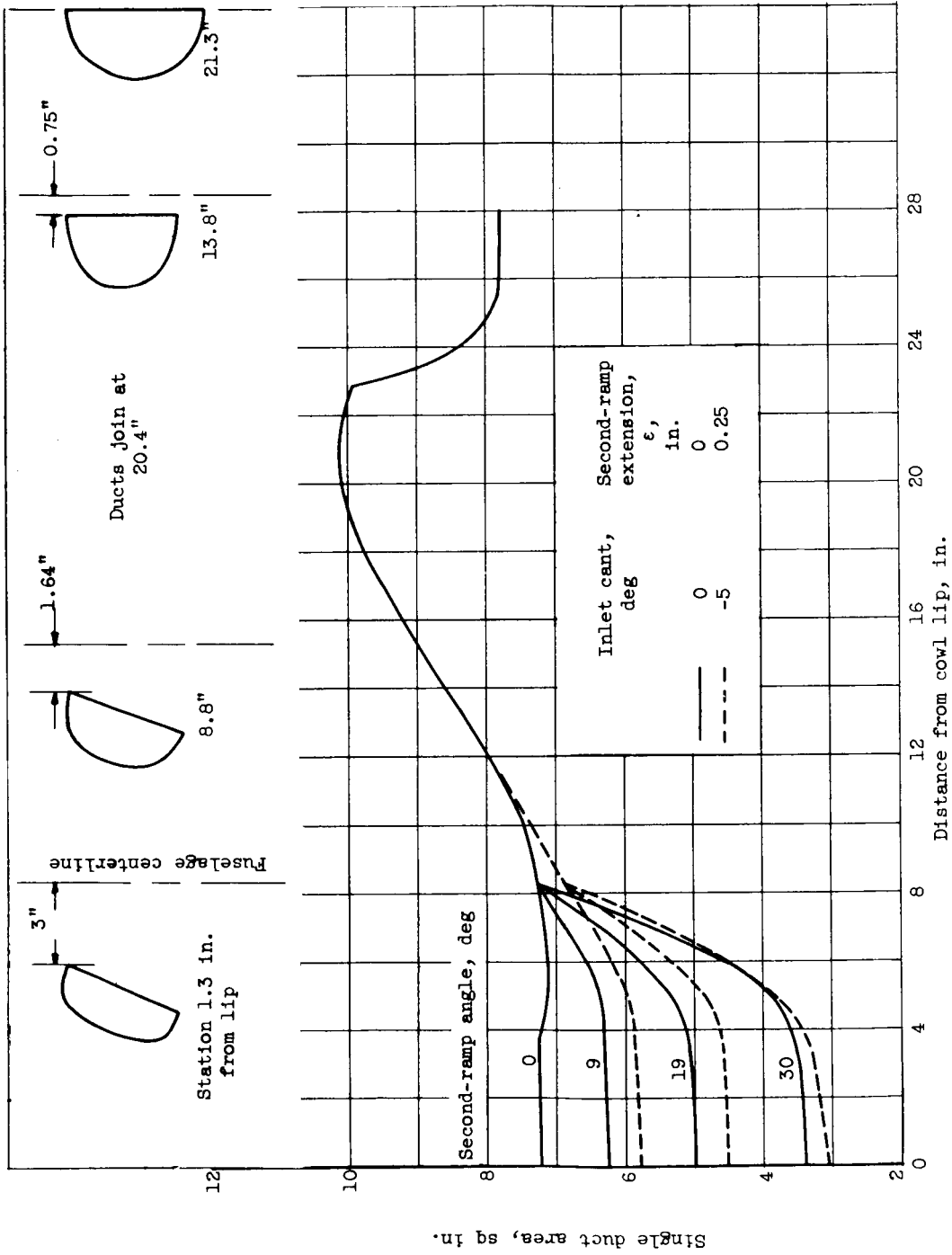
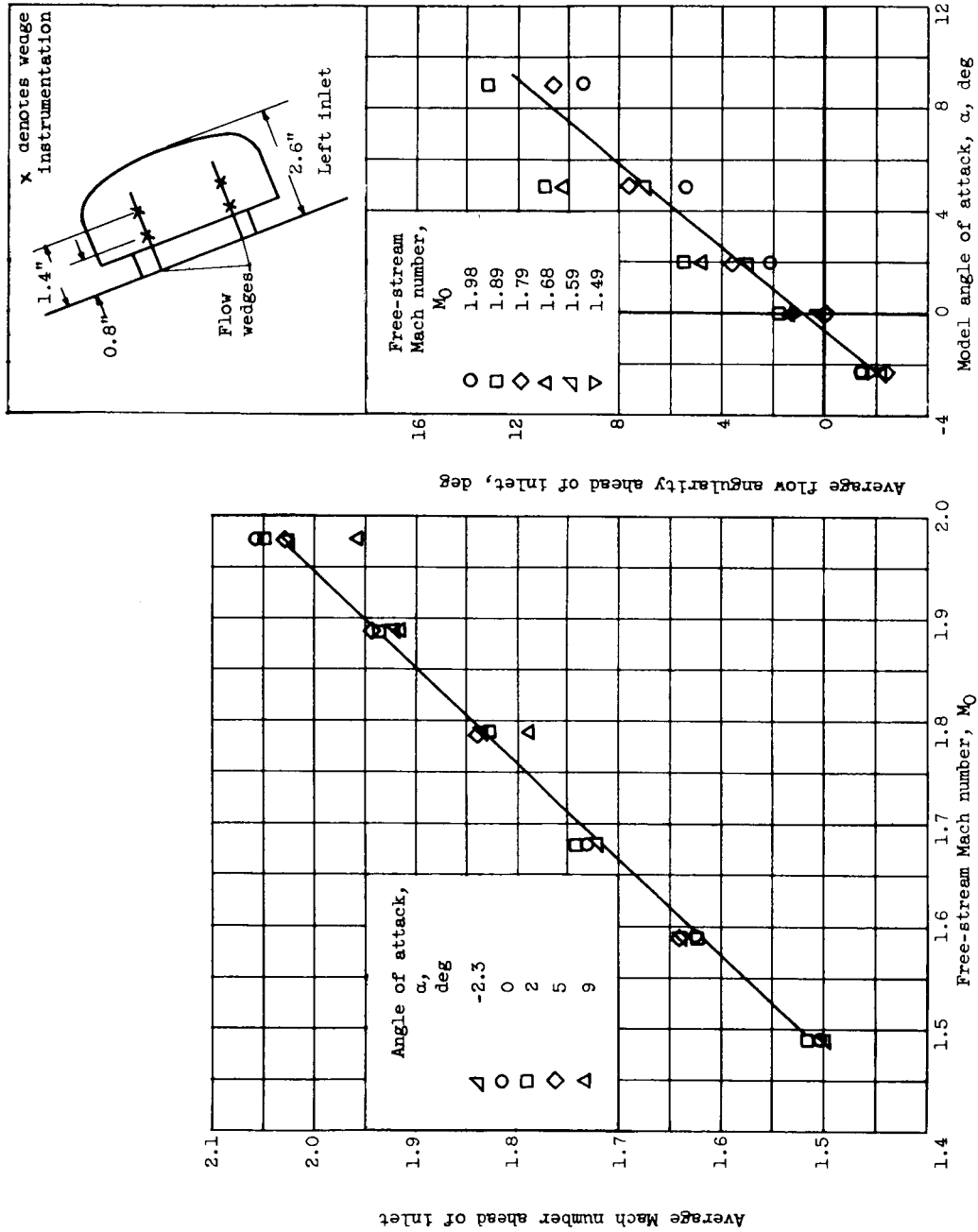
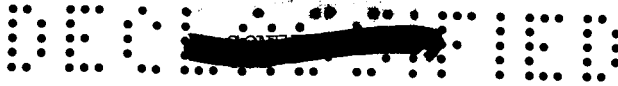


Figure 2. - Subsonic-diffuser area variation.

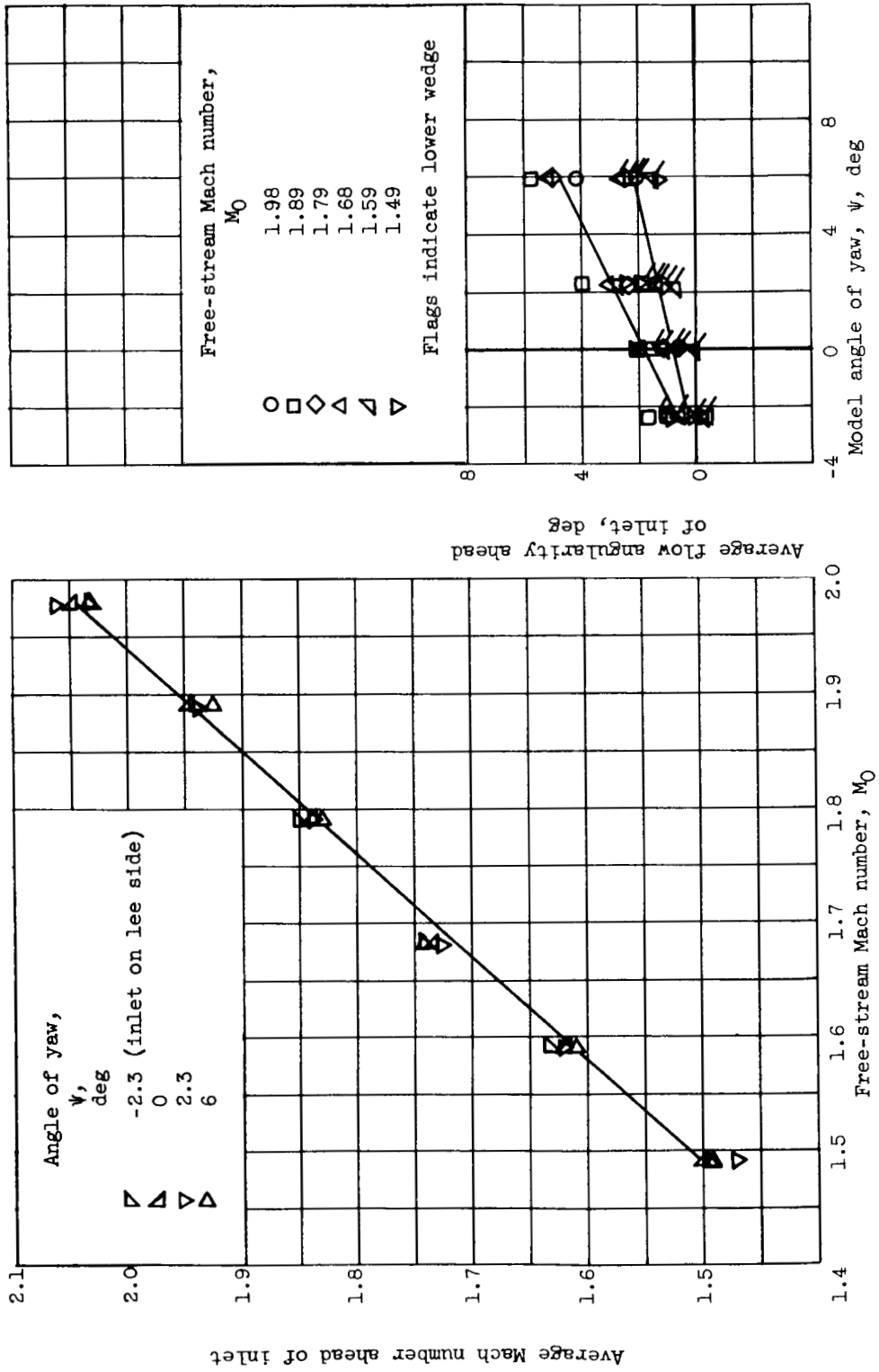
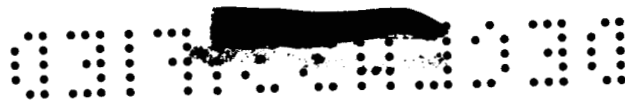


(a) Effect of angle of attack.

Figure 3. - Variation of average local Mach number and flow angularity ahead of inlet with free-stream Mach number and angles of attack and yaw.







(b) Effect of angle of yaw.

Figure 3. - Concluded. Variation of average local Mach number and flow angularity ahead of inlet with free-stream Mach number and angles of attack and yaw.

4151  
CA-3

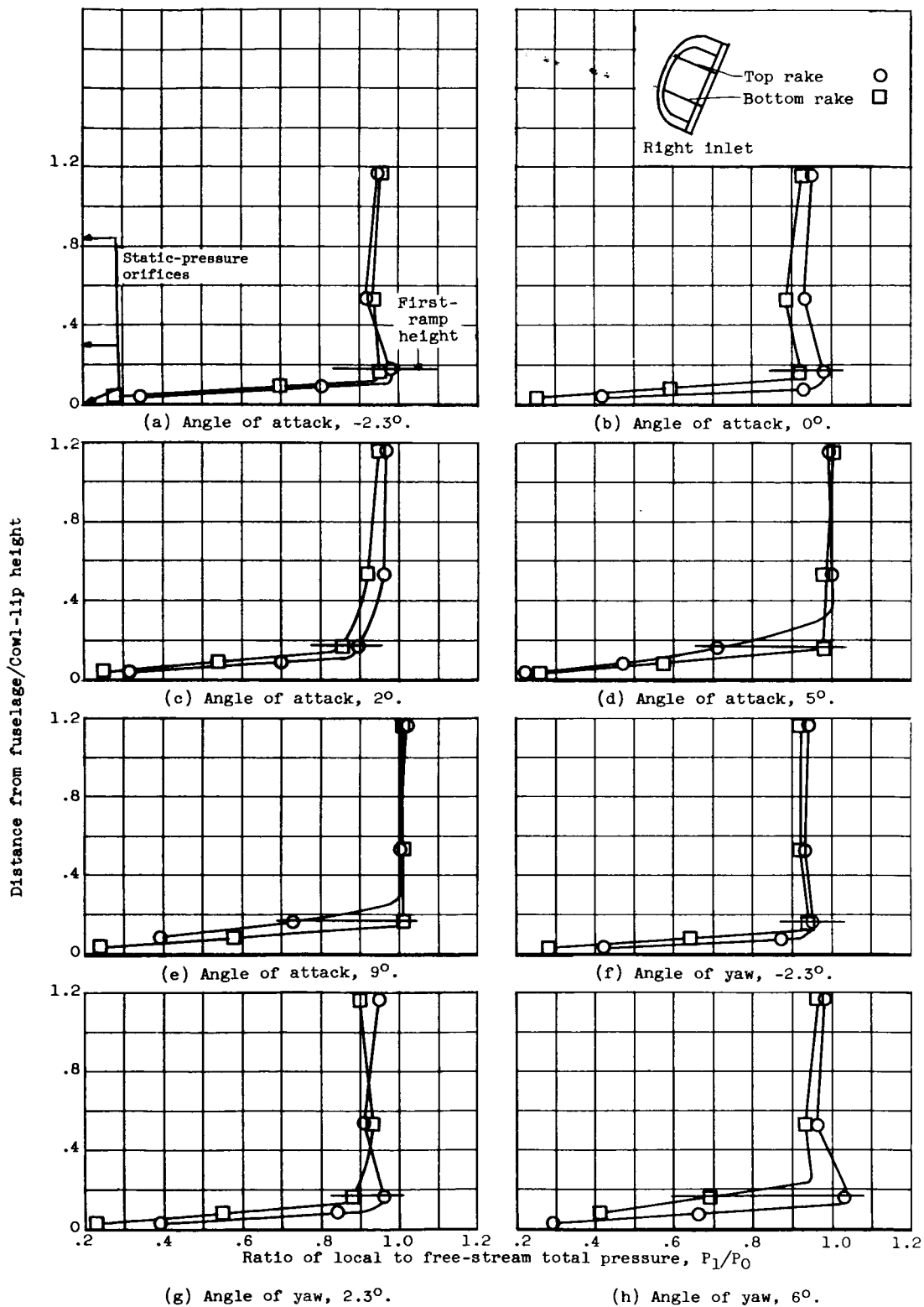
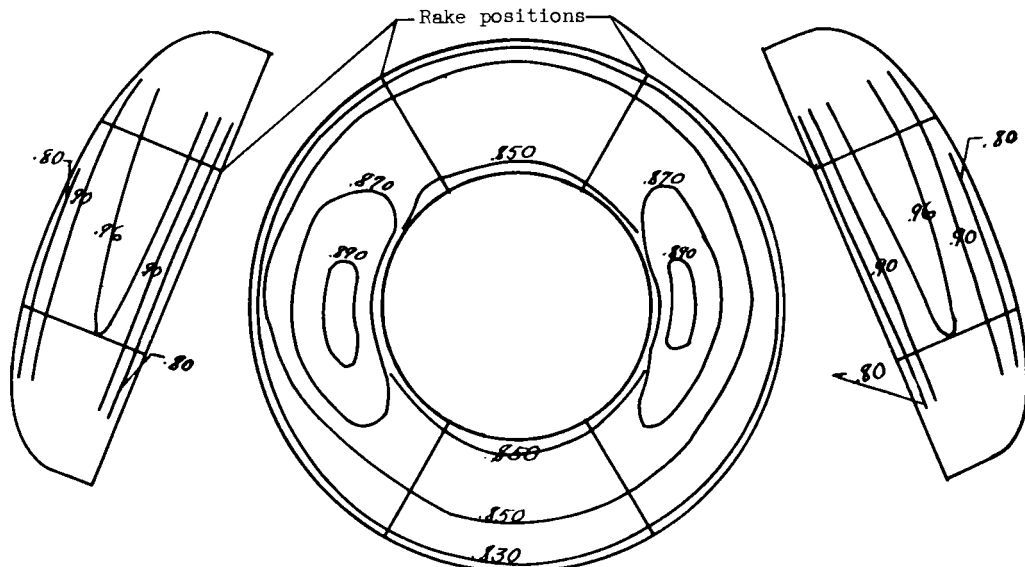
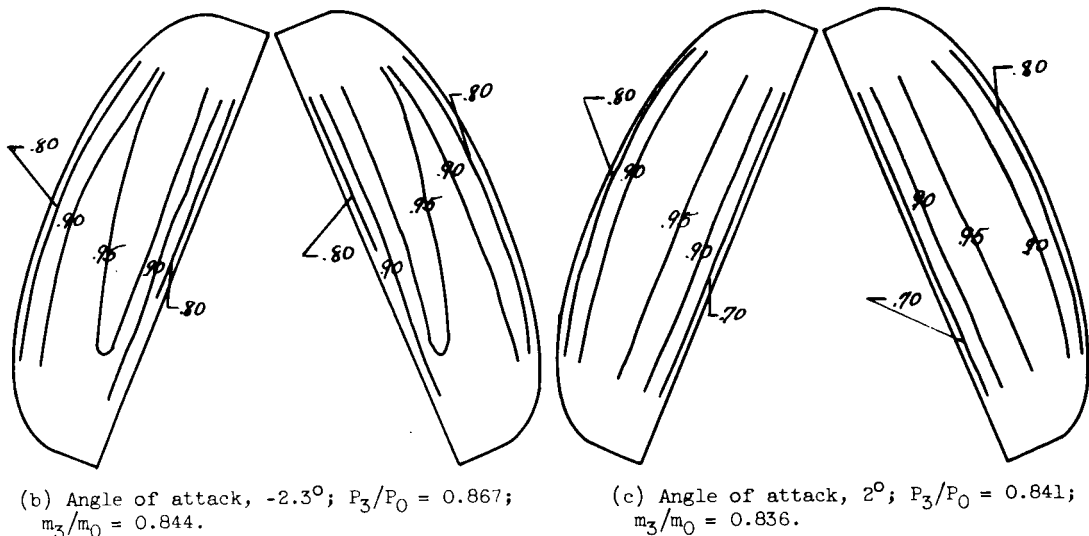


Figure 4. - Effect of model angles of attack and yaw on local total-pressure distribution ahead of inlet.



(a) Angle of attack,  $0^\circ$ ;  $P_3/P_0 = 0.860$ ;  $m_3/m_0 = 0.857$ .

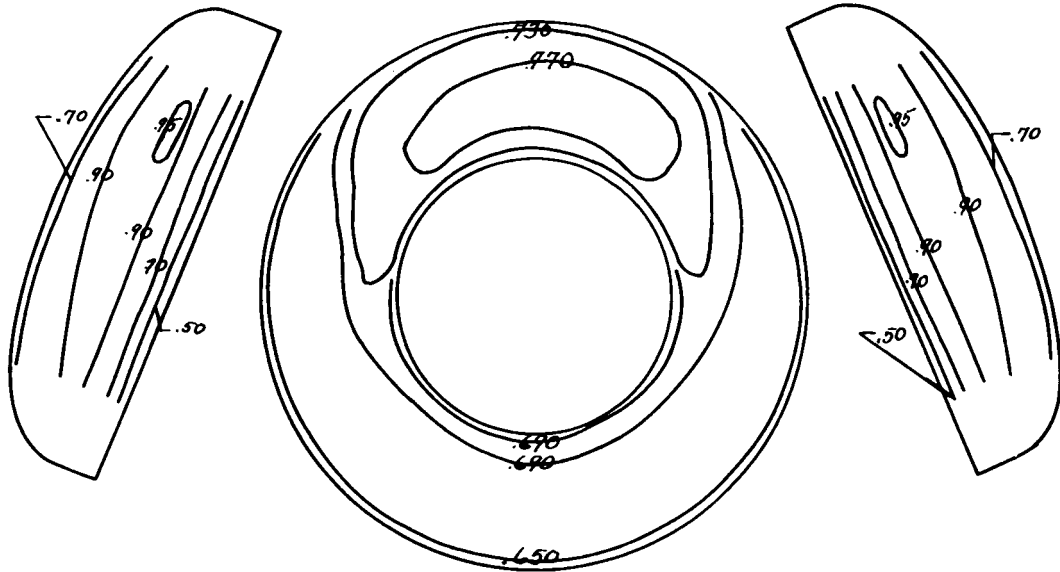


(b) Angle of attack,  $-2.3^\circ$ ;  $P_3/P_0 = 0.867$ ;  
 $m_3/m_0 = 0.844$ .

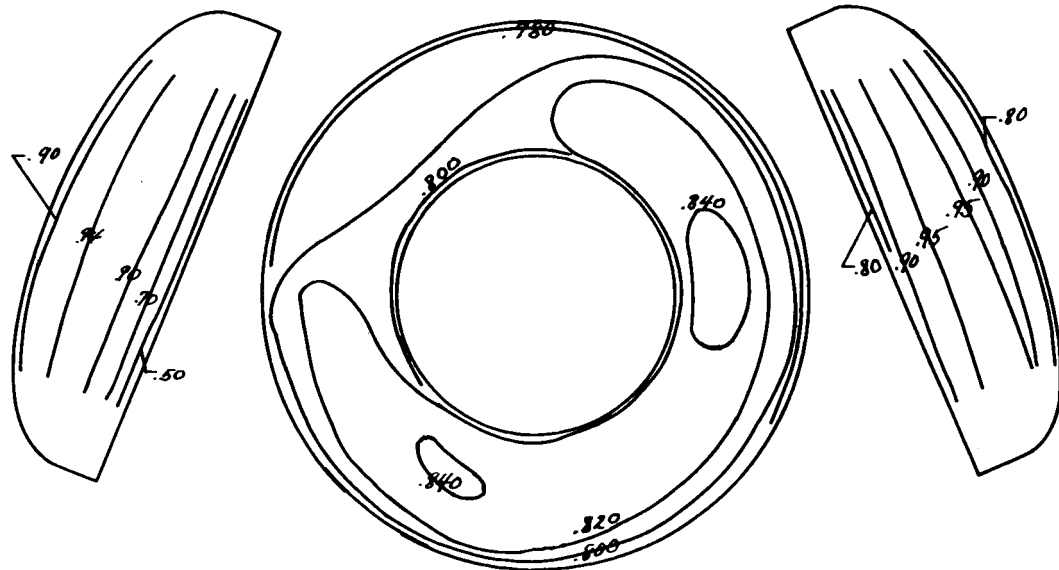
(c) Angle of attack,  $2^\circ$ ;  $P_3/P_0 = 0.841$ ;  
 $m_3/m_0 = 0.836$ .

Figure 5. - Effect of angles of attack and yaw on inlet and compressor-face profiles for  $19^\circ$  second-ramp angle at free-stream Mach number of 2.0 and  $0^\circ$  cant.





(d) Angle of attack,  $9^\circ$ ;  $P_3/P_0 = 0.709$ ;  $m_3/m_0 = 0.719$ .



(e) Angle of yaw,  $6^\circ$ ;  $P_3/P_0 = 0.821$ ;  $m_3/m_0 = 0.833$ .

Figure 5. - Concluded. Effect of angles of attack and yaw on inlet and compressor-face profiles for  $19^\circ$  second-ramp angle at free-stream Mach number of 2.0 and  $0^\circ$  cant.



CA-3 back 4151

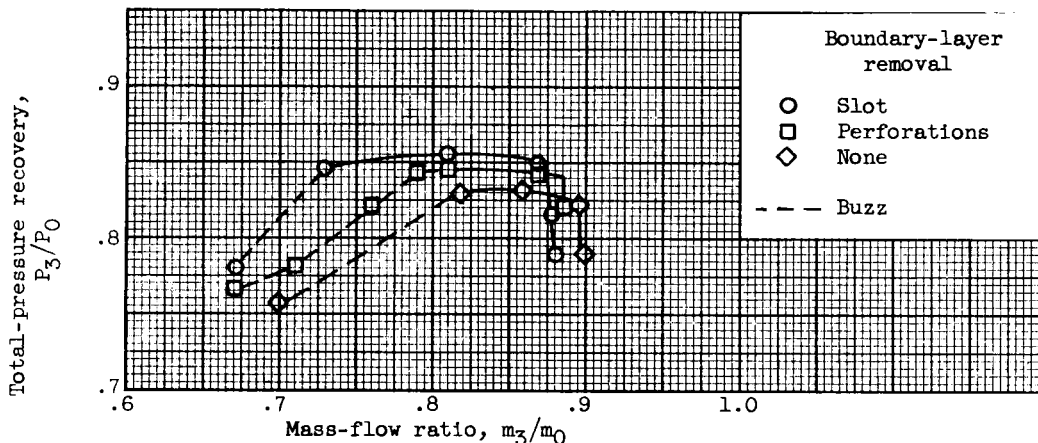
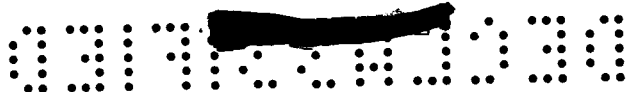


Figure 6. - Effect of compression-surface boundary-layer removal on inlet performance. Mach number, 2.0; second-ramp angle,  $19^\circ$ ; second-ramp extension, 0; angle of attack,  $2^\circ$ ; cant,  $0^\circ$ .

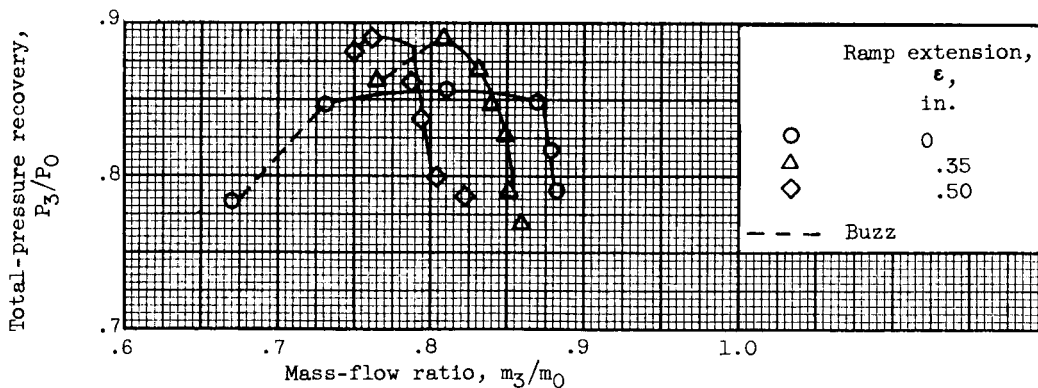
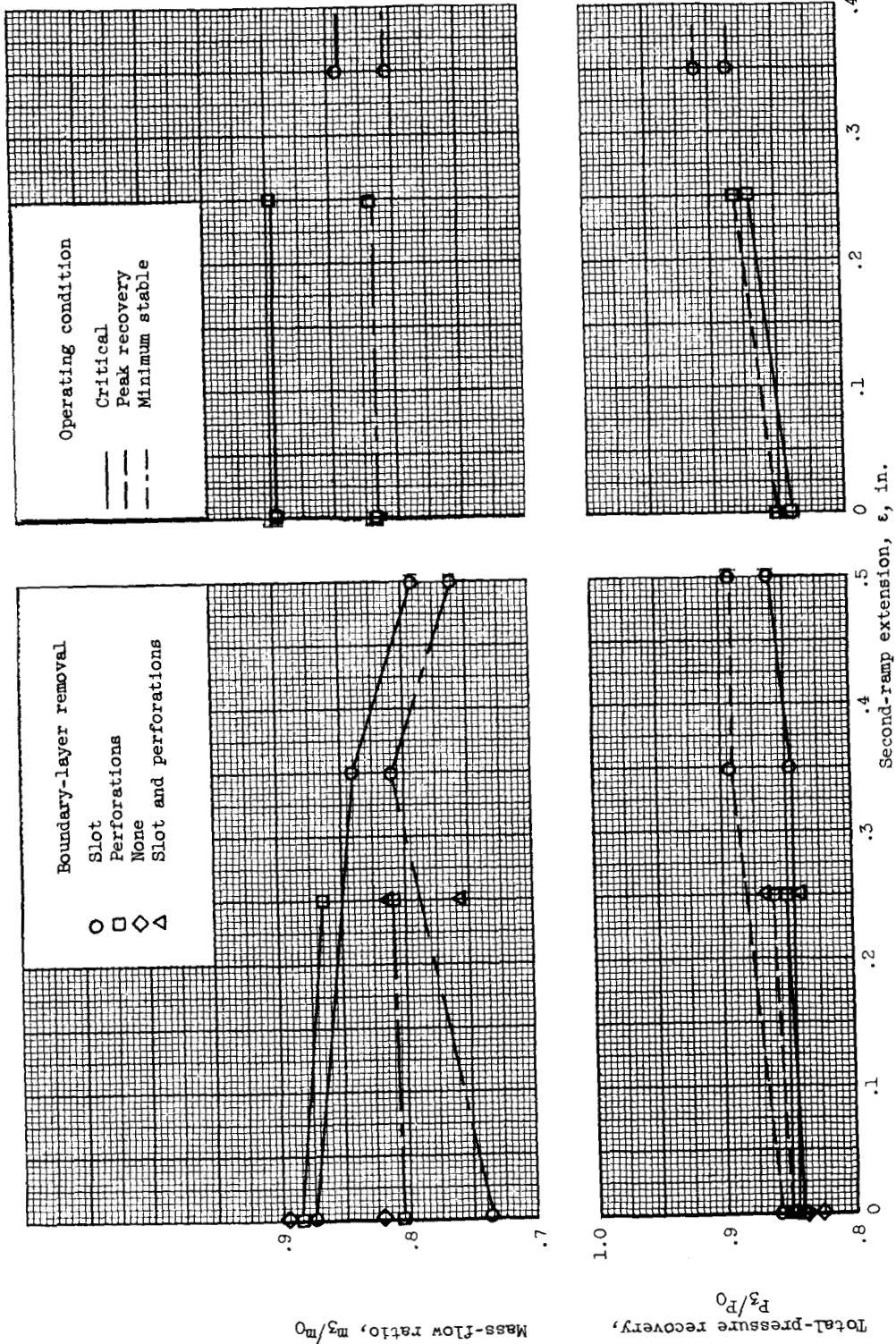


Figure 7. - Effect of second-ramp extension on inlet performance. Mach number, 2.0; second-ramp angle  $19^\circ$ ; slot boundary-layer removal; angle of attack,  $2^\circ$ ; cant,  $0^\circ$ .



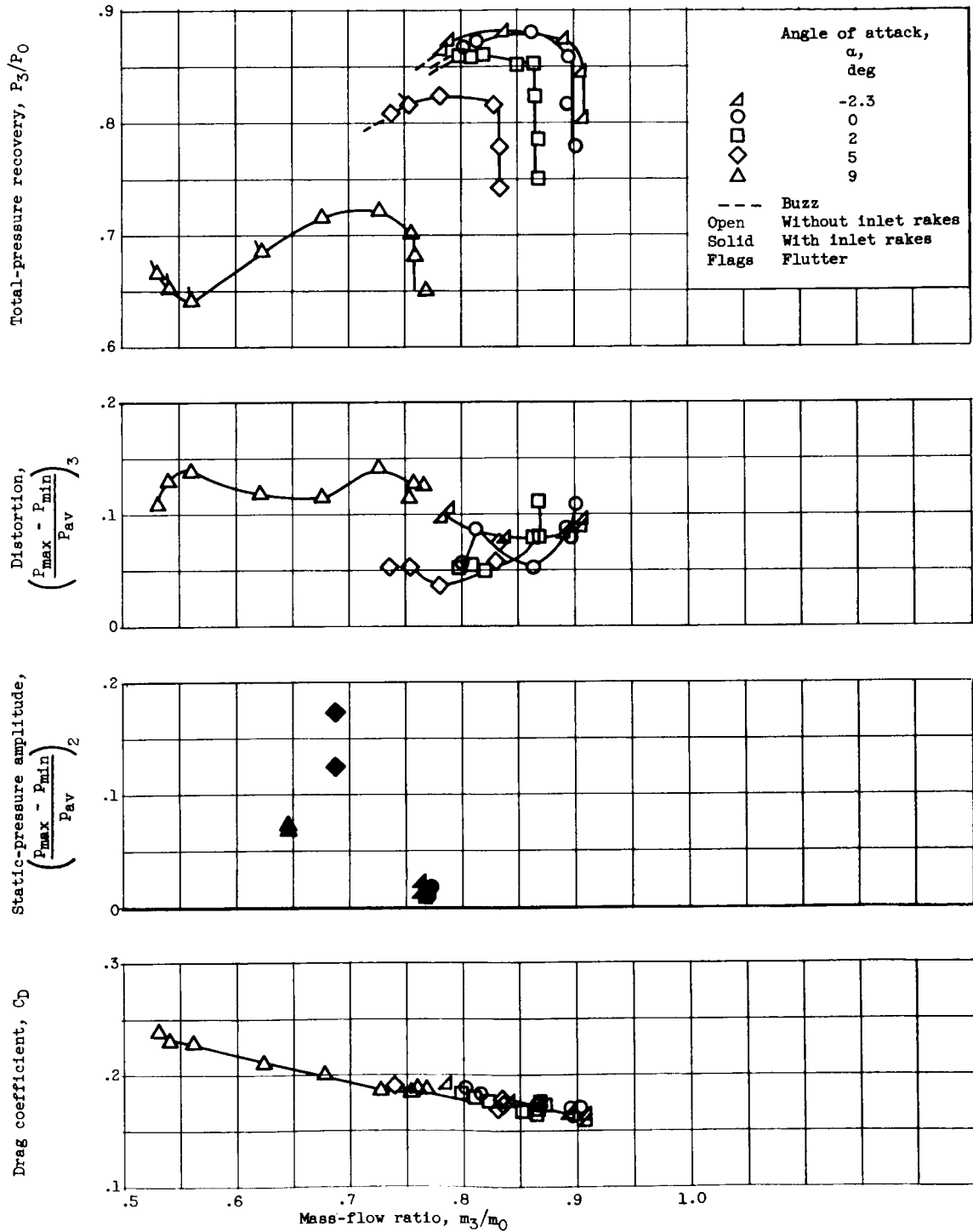
4151



(a) Angle of attack, 20°. (b) Angle of attack, 0°. Figure 8. - Summary of effects of compression-surface boundary-layer-removal systems and second-ramp extension on inlet performance. Mach number, 2.0; second-ramp angle, 19°; cant, 0°.



4151

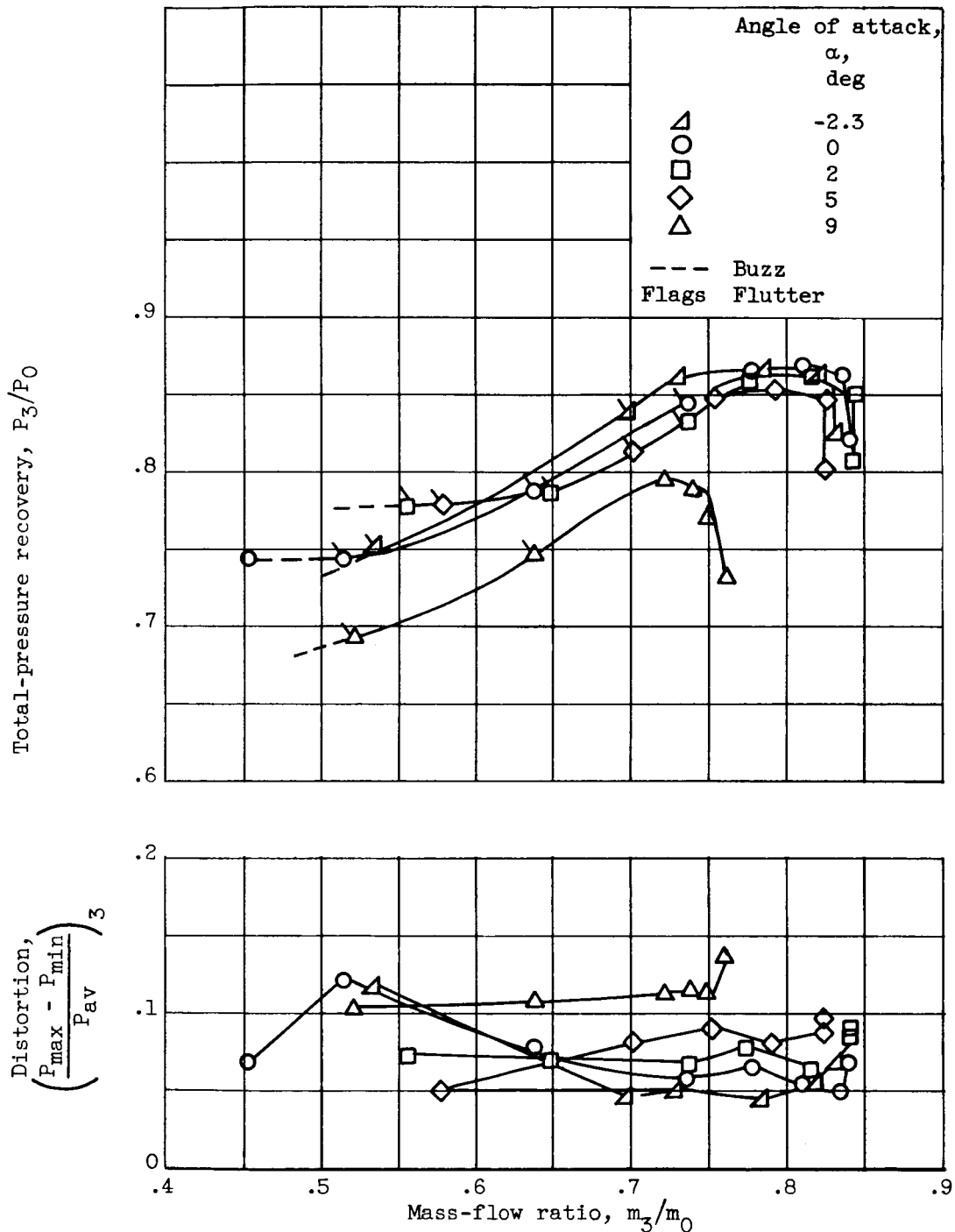


(a) Mach number, 2.0; second-ramp angle, 19°; cant, 0°.

Figure 9. - Effect of cant on angle-of-attack performance.



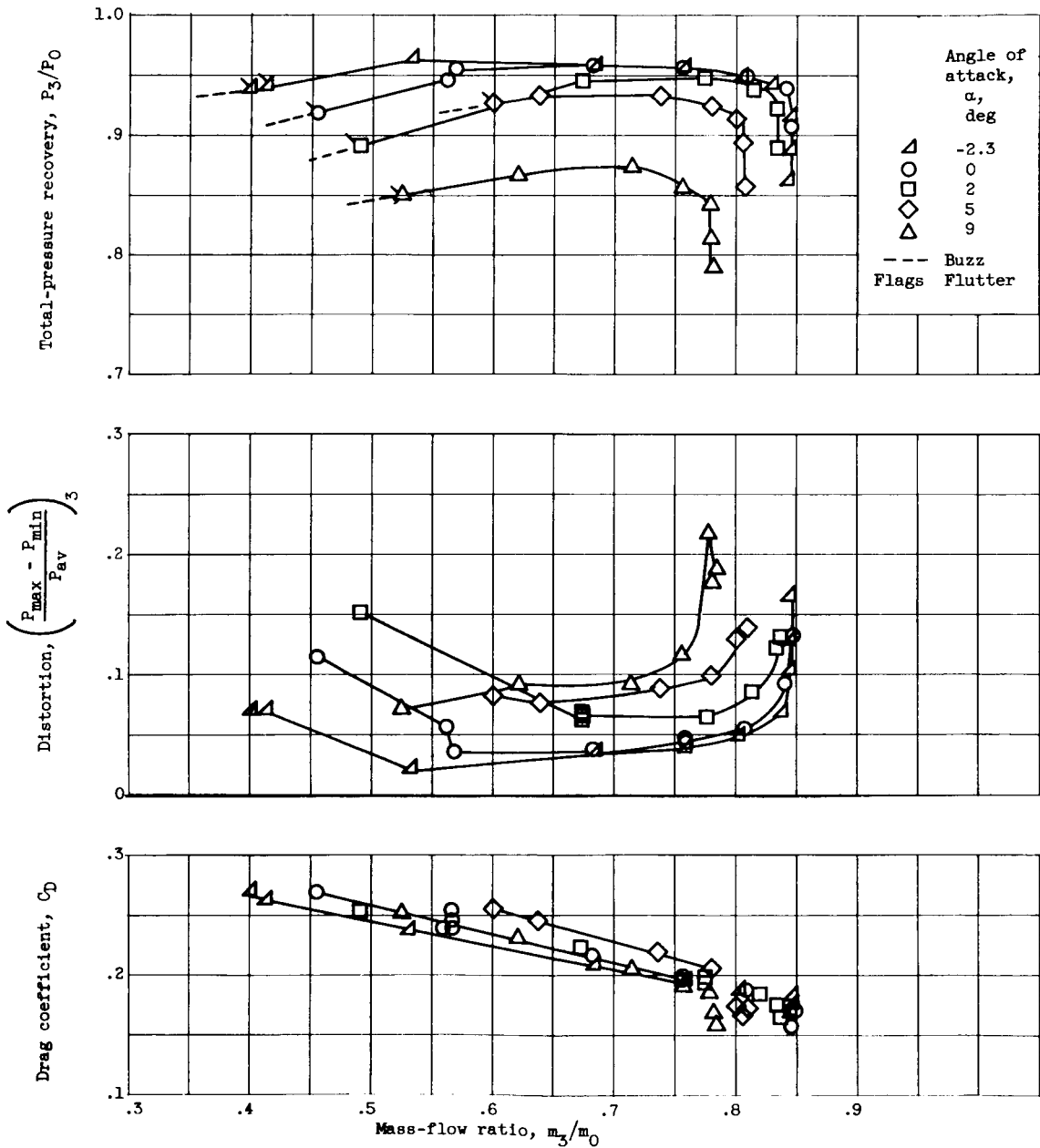
4151



(b) Mach number, 2.0; second-ramp angle,  $19^\circ$ ; cant,  $-5^\circ$ .

Figure 9. - Continued. Effect of cant on angle-of-attack performance.



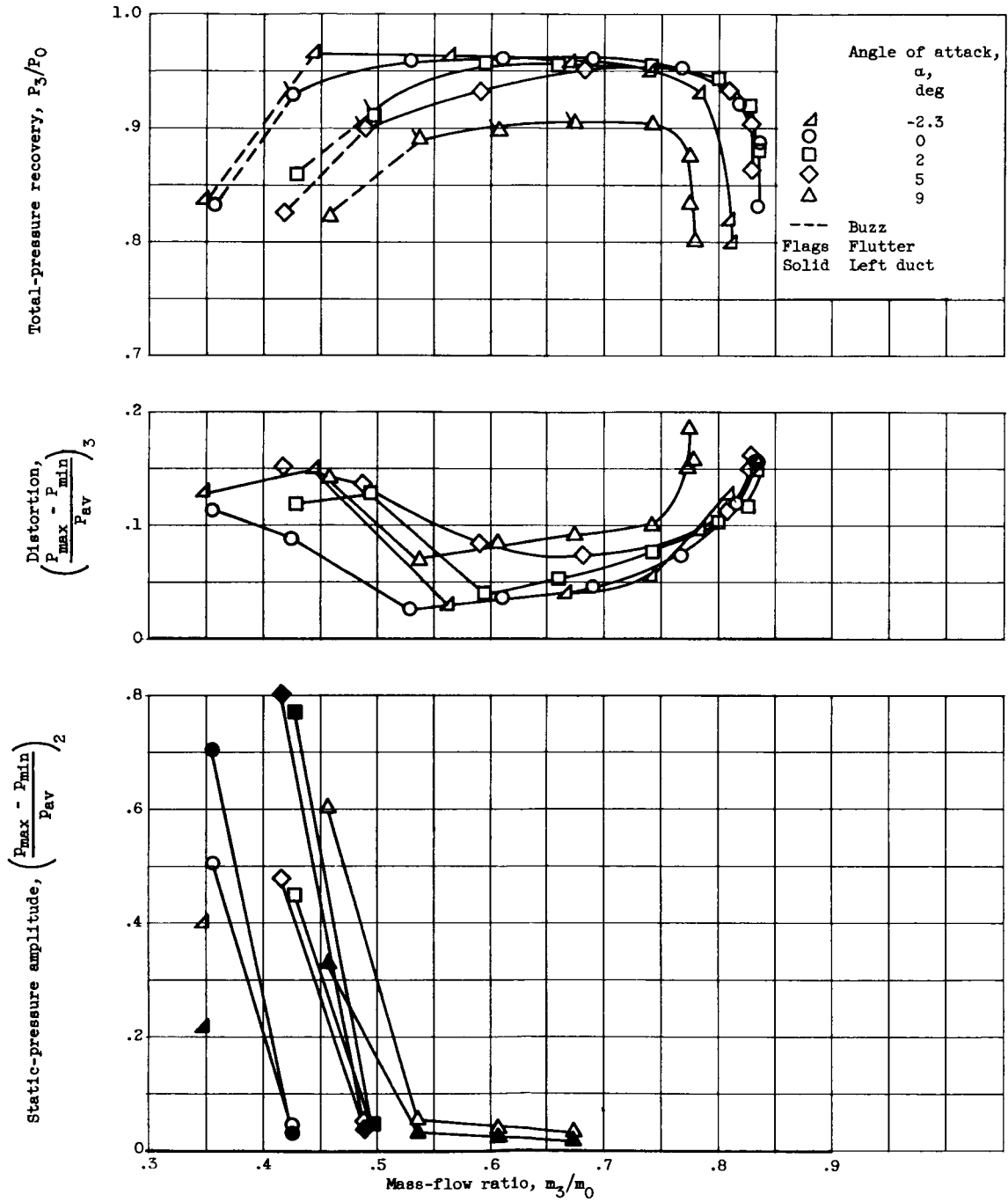


(c) Mach number, 1.5; second-ramp angle,  $90^\circ$ ; cant,  $0^\circ$ .

Figure 9. - Continued. Effect of cant on angle-of-attack performance.



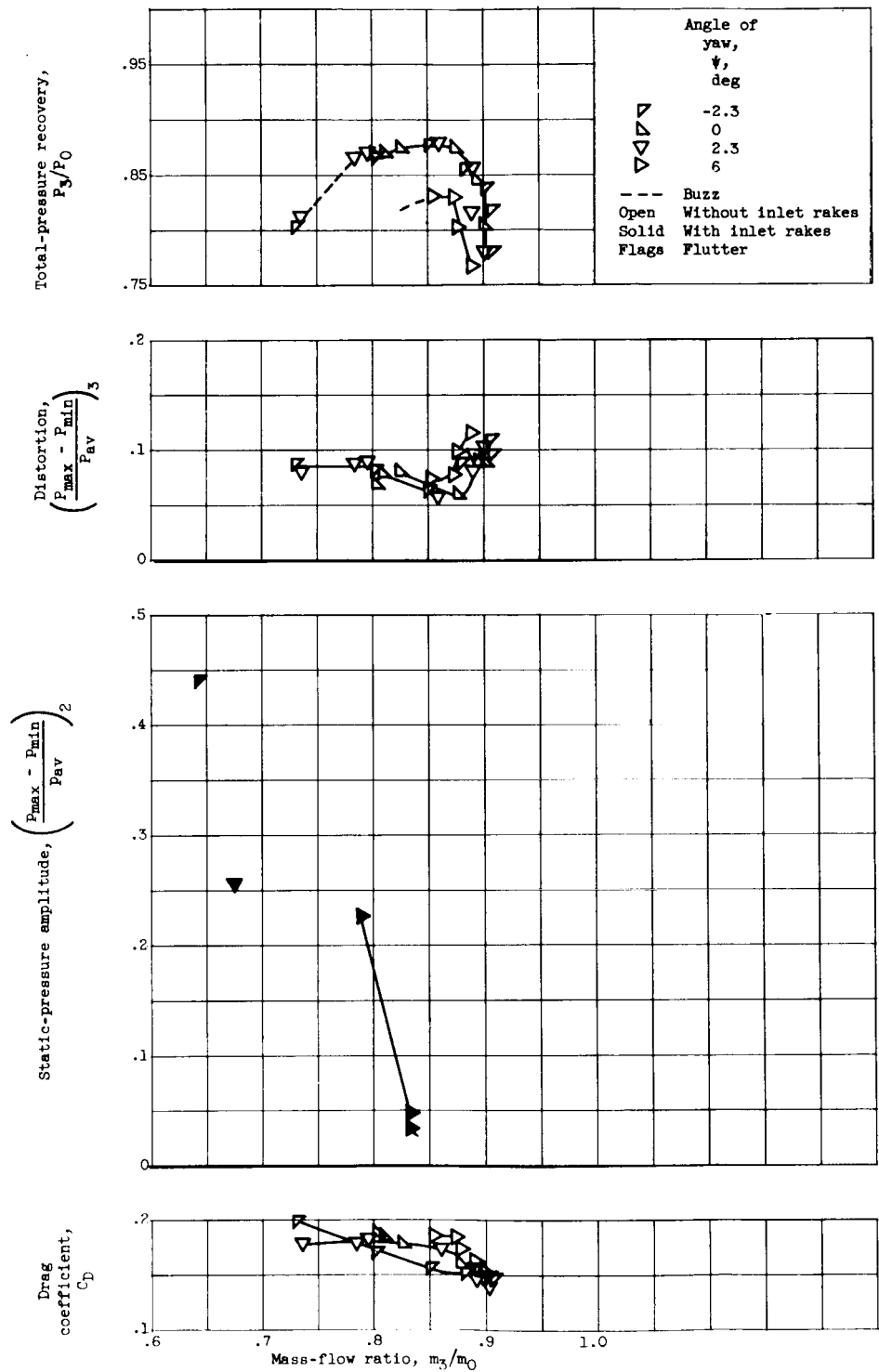
DECLASSIFIED



(d) Mach number, 1.5; second-ramp angle,  $9^\circ$ ; cant,  $-5^\circ$ .

Figure 9. - Concluded. Effect of cant on angle-of-attack performance.

DECLASSIFIED



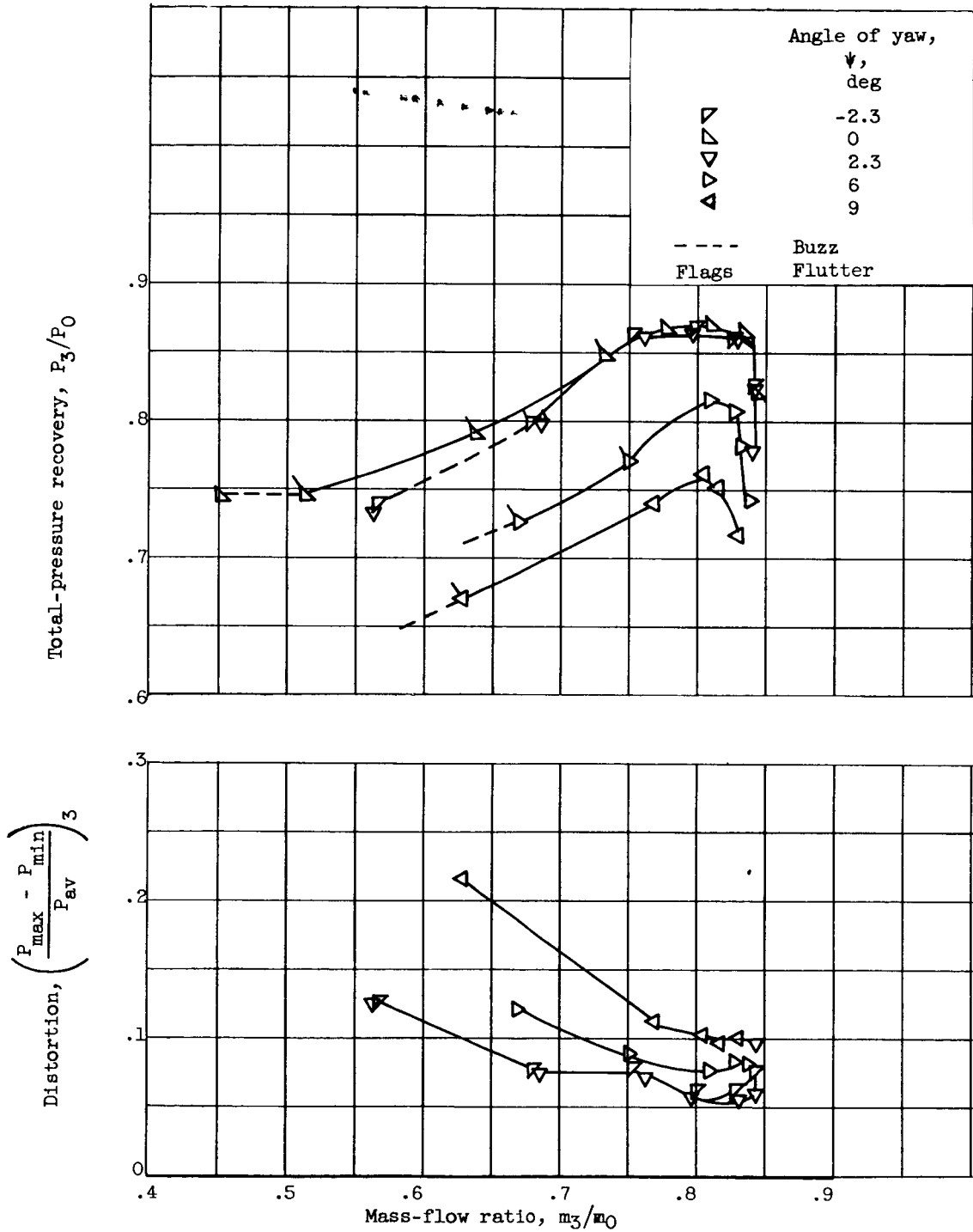
(a) Cant,  $0^\circ$ .

Figure 10. - Effect of cant on angle-of-yaw performance. Mach number, 2.0; second-ramp angle,  $19^\circ$ .



4151

CA-4 back  
4151



(b) Cant,  $-5^\circ$ .

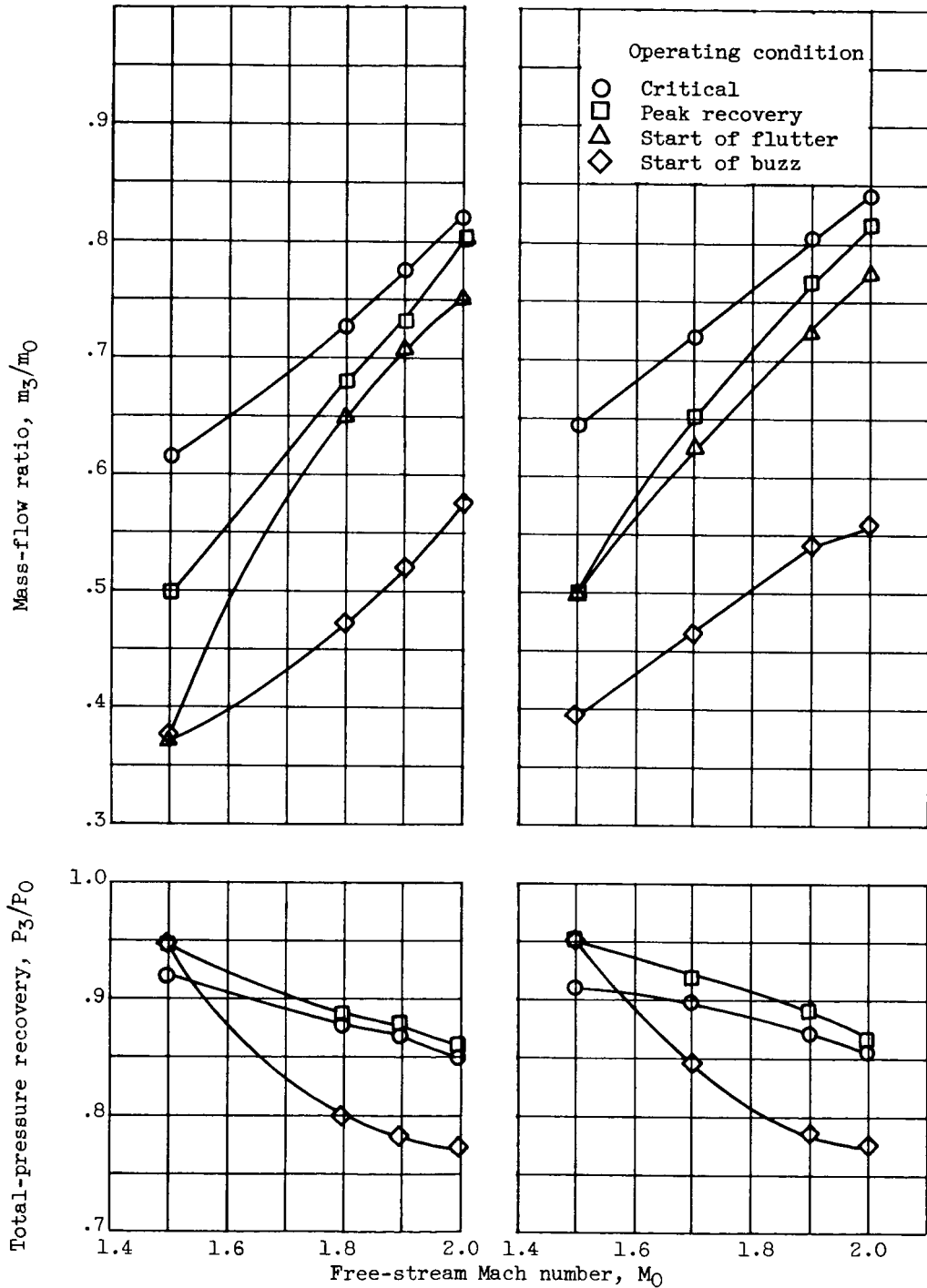
Figure 10. - Concluded. Effect of cant on angle-of-yaw performance. Mach number, 2.0; second-ramp angle,  $19^\circ$ .







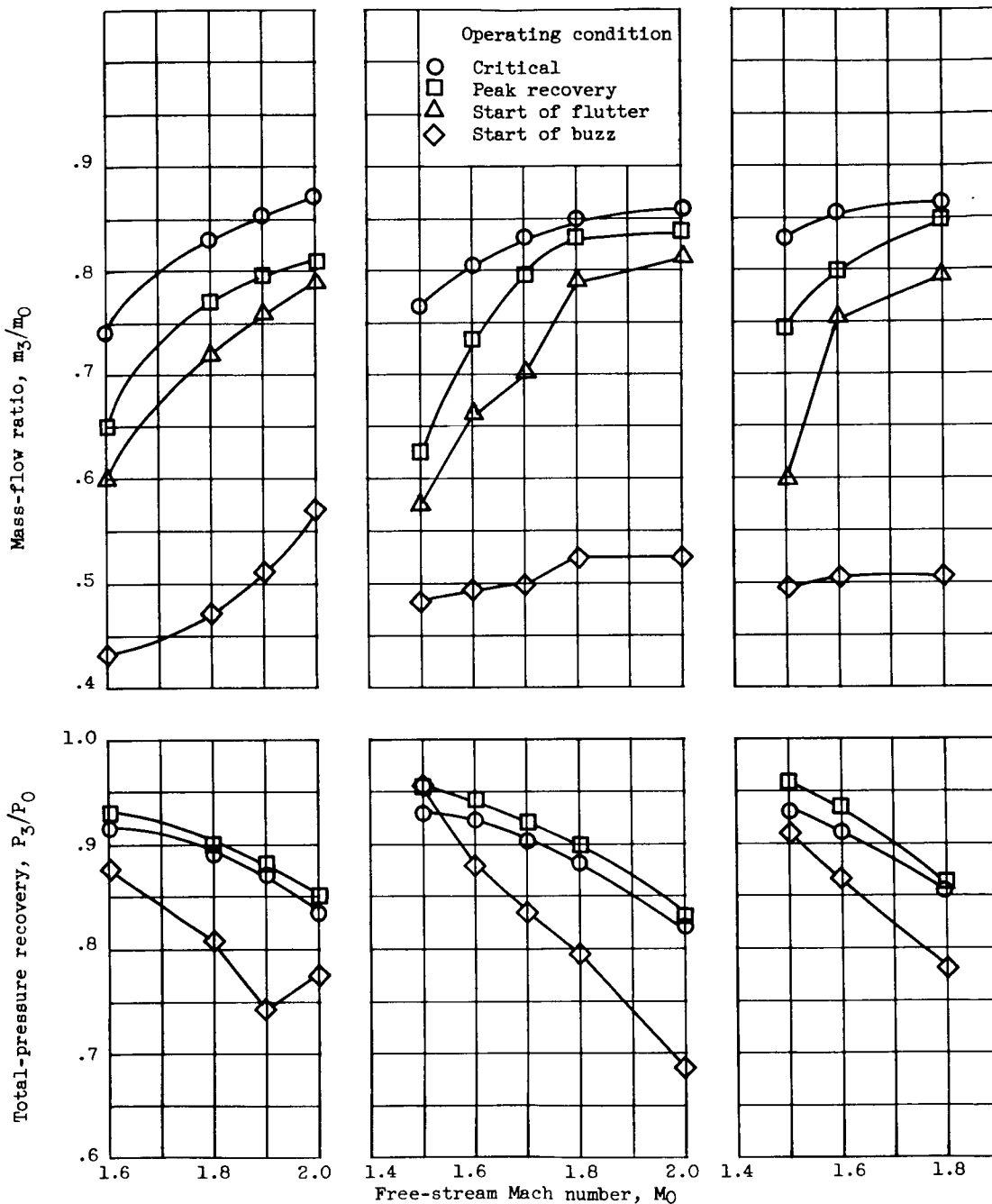
4151



(a) Second-ramp angle, 21°; cant, -5°. (b) Second-ramp angle, 19°; cant, -5°.

Figure 12. - Performance variations with free-stream Mach number for fixed second-ramp angles. Angle of attack, 2°.





(c) Second-ramp angle,  $17^\circ$ ; cant,  $-5^\circ$ .

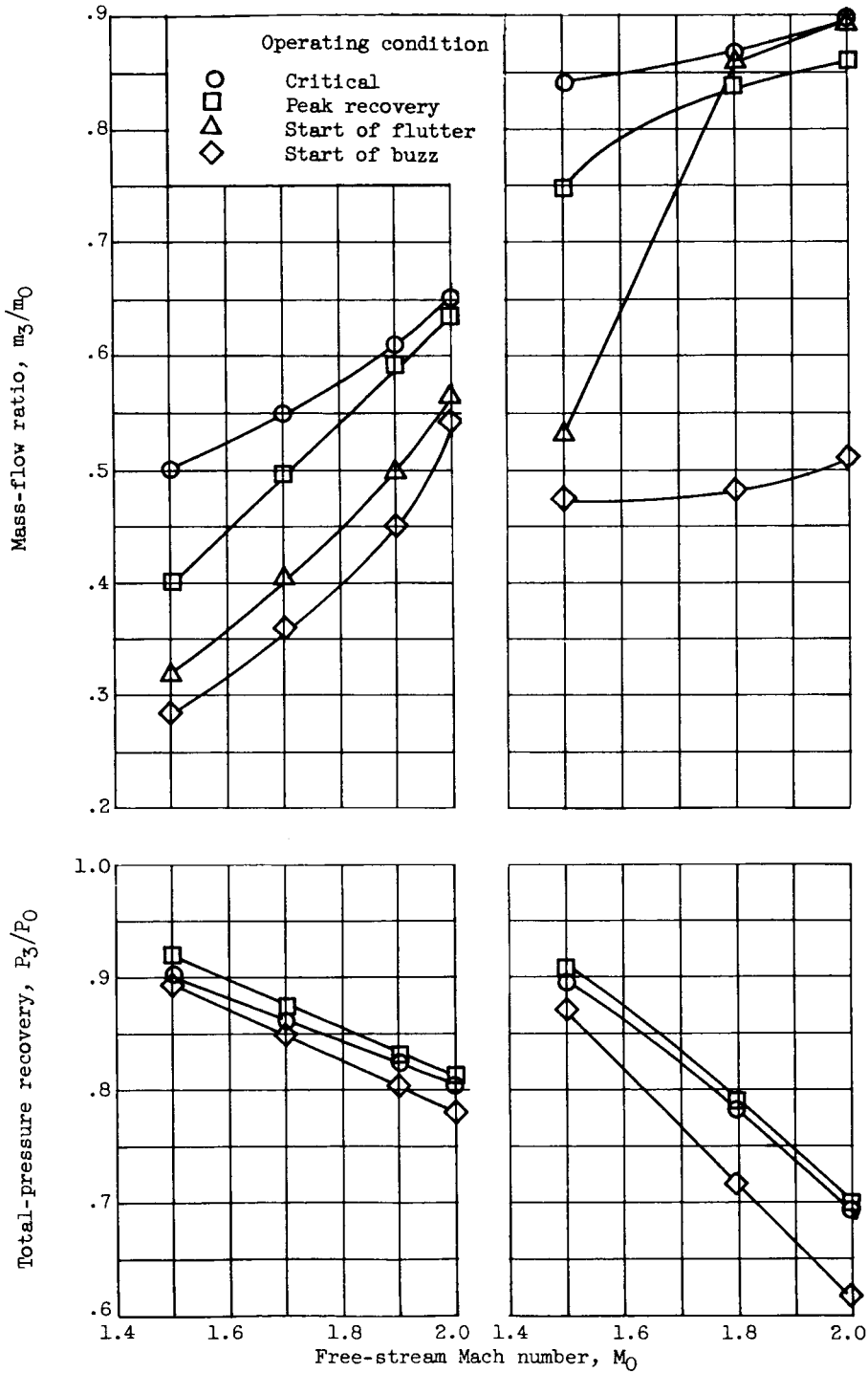
(d) Second-ramp angle,  $13^\circ$ ; cant,  $-5^\circ$ .

(e) Second-ramp angle,  $9^\circ$ ; cant,  $-5^\circ$ .

Figure 12. - Continued. Performance variations with free-stream Mach number for fixed second-ramp angles. Angle of attack,  $2^\circ$ .



4151



(f) Second-ramp angle,  $30^\circ$ ; cant,  $0^\circ$ .

(g) Second-ramp angle,  $0^\circ$ ; cant,  $0^\circ$ .

Figure 12. - Concluded. Performance variations with free-stream Mach number for fixed second-ramp angles. Angle of attack,  $2^\circ$ .



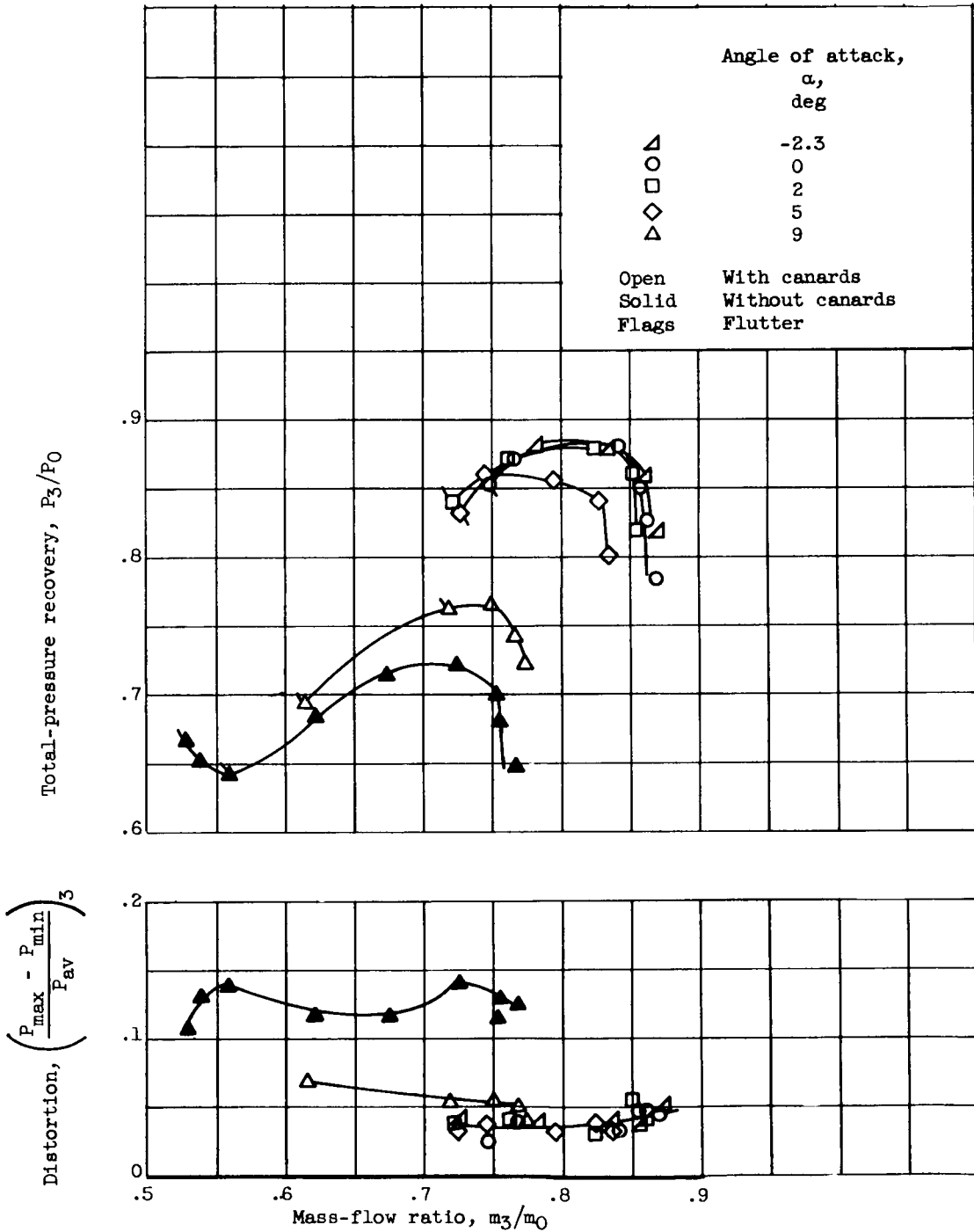


Figure 13. - Inlet performance with canards mounted on fuselage nose. Mach number, 2.0; second-ramp angle,  $19^\circ$ ; cant,  $0^\circ$ .

